PCCP

Accepted Manuscript

ROYAL SOCIETY OF CHEMISTRY

www.rsc.org/pccp

PCCP Guidelines for Referees

Physical Chemistry Chemical Physics **(*PCCP*) is a high quality journal with a large international readership from many communities**

Only very important, insightful and high-quality work should be recommended for publication in *PCCP*.

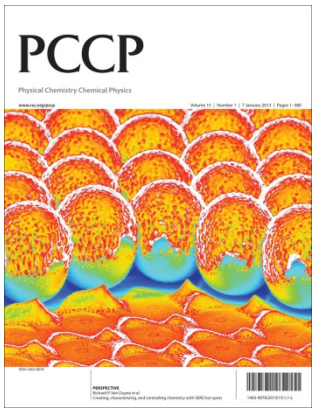

To be accepted in *PCCP* - a manuscript must report:

- Very high quality, reproducible new work
- **Important new physical insights** of significant general interest
- A novel, stand-alone contribution

Routine or incremental work should not be recommended for publication. Purely synthetic work is not suitable for PCCP

If you rate the article as 'routine' yet recommend acceptance, please give specific reasons in your report.

Less than 50% of articles sent for peer review are recommended for publication in *PCCP*. The current PCCP Impact Factor is 3.83

PCCP is proud to be a leading journal. We thank you very much for your help in evaluating this manuscript. Your advice as a referee is greatly appreciated.

With our best wishes,

Philip Earis (pccp@rsc.org)
Managing Editor, PCCP

Prof Daniella Goldfarb
Chair, PCCP Editorial Board

General Guidance (For further details, see the RSC's Refereeing Procedure and Policy)

Referees have the responsibility to treat the manuscript as confidential. Please be aware of our **Ethical Guidelines** which contain full information on the responsibilities of referees and authors.

When preparing your report, please:
• Comment on the originality, importance, impact and scientific reliability of the work;
• State clearly whether you would like to see the paper accepted or rejected and give detailed comments (with references) that will both help the Editor to make a decision on the paper and the authors to improve it;

Please inform the Editor if:
• There is a conflict of interest;
• There is a significant part of the work which you cannot referee with confidence;
• If the work, or a significant part of the work, has previously been published, including online publication, or if the work represents part of an unduly fragmented investigation.

When submitting your report, please:
• Provide your report rapidly and within the specified deadline, or inform the Editor immediately if you cannot do so. We welcome suggestions of alternative referees.

Physical Chemistry Chemical Physics RSCPublishing

ARTICLE

Nanoparticle Dispersion in Polymer Nanocomposites by Spin-Diffusion-Averaged Paramagnetic Enhanced NMR Relaxometry: Scaling Relations and Applications

Bo Xu,[a]* Johannes Leisen [b] and Haskell W. Beckham [a]*

Scaling relationships are identified between NMR longitudinal relaxation times and clay dispersion quality in polymer/paramagnetic clay nanocomposites. Derived from a previously published analytical relationship developed from a lamella-based model, the scaling relationships are based on the enhancement of NMR relaxation rates with increasing exfoliation and dispersion homogeneity. The paramagnetic contribution to the NMR relaxation rate is inversely proportional to the square of clay interparticle spacing, and directly proportional to clay weight fraction squared. These scaling relationships allow the prediction of relative exfoliation of clay particles for a given series of polymer/clay nanocomposites. With independent knowledge of clay exfoliation in a single sample (*e.g.*, from transmission electron microscopy), NMR relaxometry data may be converted into absolute measures of exfoliation. These scaling relations are confirmed with samples of fully exfoliated poly(vinyl alcohol)/montmorillonite nanocomposites, and then used to reveal exfoliation and dispersion quality in a series of nylon-6/montmorillonite nanocomposites. This characterization route is advantageous because NMR relaxometry can more rapidly provide clay dispersion information that is averaged over larger sample volumes than transmission electron microscopy.

Introduction

Polymer properties can be significantly enhanced when nanoscopic fillers are introduced to the matrix.[1-11] Among the most common inorganic fillers are clay particles, best described as stacks of platelets in which platelets are 1-nm thick with lateral dimensions of hundreds of nanometers.[12, 13] Platelets can be delaminated from stacks by exfoliation so that clay particles may be characterized by the number of platelets per stack. The degree to which platelet stacks are exfoliated and dispersed in matrices is governed by interfacial interactions and processing. Thus, the number of particles for a given clay loading depends on the degree of exfoliation. High clay loadings tend to give more aggregates of unexfoliated stacks. The ultimate physical properties of polymer-clay nanocomposites (PCNs) depend on the clay loading and the degree of exfoliation, or more precisely on the distribution of interparticle spacings, referred to as the dispersion. Optimization of PCN properties is facilitated by quantitative characterization of the loading-dependent exfoliation.

Characterization of clay particle morphology in terms of degree of exfoliation and dispersion homogeneity can be accomplished by solid-state NMR relaxometry when clay platelets contain paramagnetic impurities that increase spin-lattice relaxation rate, $1/T_1$, of the matrix polymer.[14-17] We recently published an analytical relationship between longitudinal nuclear magnetic relaxation and interparticle spacings (IPS) in polymer/paramagnetic clay nanocomposites.[18] Using data collected with ^{1}H NMR relaxometry, we quantified clay nanoparticle dispersion in some equi-biaxially stretched polypropylene-montmorillonite nanocomposites, which agreed with interparticle-spacing distributions determined by statistical analysis of TEM images. Moreover, the NMR data to some extent reflected the overall quality of clay dispersion in the bulk materials. Overall, the findings revealed how clay dispersion evolved with stretching for a set of polymer-clay nanocomposites containing the same clay content. The question remains as to how the characterization method and analysis behaves for PCNs with varying clay loadings.

In this study, we present some scaling relations derived from the analytical expression connecting NMR longitudinal relaxation with clay content and dispersion. More specifically, we show how the paramagnetic contribution to the spin-lattice relaxation rate scales with the inverse interparticle separation squared and with the clay content. We confirm the validity of the scaling relations on a series of fully exfoliated 'model' poly(vinyl alcohol) (PVA)/ montmorillonite (MMT) nanocomposites prepared by a solution-intercalation film-casting method.[19, 20] We then demonstrate their applicability on a series of technically relevant nylon-6/MMT nanocomposites containing up to 20 wt% clay.[21] In doing so, we introduce a new method for quantifying and visualizing clay dispersion in PCNs with respect to average interparticle spacing and the number of platelets/stack per particle.

Experimental Details

Montmorillonite (MMT) STx-1b (1.2 wt% Fe_2O_3 as Fe^{3+})[22] was obtained from the Source Clays Repository, Purdue University, Indiana. Poly(vinyl alcohol) (PVA) (M_w = 31–50 kg/mol, 98–99% hydrolyzed, Sigma–Aldrich) was used as received. PVA/MMT_{STx-1b} nanocomposites (PVA/MMT_{STx-1b}) were prepared at weight ratios (PVA/MMT_{STx-1b}) of 100/1, 100/2, 100/4, 100/6, 100/8, and 100/10 by a solution-intercalation film-casting method as described by others.[19, 20] The samples were dried under vacuum at 80 °C for 48

hours prior to any measurements. Octadecylamine (C18) was used as received from Sigma–Aldrich. Octadecylamine (C18)-modified $MMT_{STx\text{-}1b}$ was prepared by cation exchange using a C18 amount equal to the cation exchange capacity (CEC) of STx-1b (CEC = 84.4 mequiv/100 g), as described elsewhere.[23]

Details of the ^{1}H NMR relaxation measurements were reported previously.[14,31] In brief, ^{1}H saturation-recovery NMR experiments were conducted at room temperature using a two-channel 7-mm magic-angle spinning (MAS) probe in a Bruker DSX-300 solid-state NMR spectrometer (300 MHz, 7.05 T). All relaxation measurements were made without sample spinning in the MAS probe.[16, 24]

Wide-angle X-ray scattering was conducted on a PANalytical X'Pert PRO diffractometer using Cu $K\alpha_1$ radiation generated at 45 kV and 40 mA (wavelength λ = 1.5406 Å). Samples were scanned at 0.02°/s in the range of 2θ =2° – 15°. The d_{001} basal spacing was calculated using the Bragg equation, $\lambda = 2d_{001}\sin\theta$.

NMR relaxometry and TEM data were taken from the literature for nylon 6/montmorillonite nanocomposites prepared by melt compounding.[21, 25] The organically modified montmorillonite in nylon 6 is Cloisite 20A (3.11 wt% Fe_2O_3 as Fe^{3+}) from Southern Clay Products, TX. The Fe_2O_3 content in Cloisite 20A was determined using elemental analysis by Southern Clay Products and corresponds to 5 wt% in the pure montmorillonite. Volume fractions of clay were calculated using specific densities of 1.3, 1.13, and 2.6 g/cm^3 for PVA, nylon 6 and neat MMT, respectively.

Results and Discussion

Model Background and Scaling Relations

Consider a regular, repeating lamellar structure of alternating clay particles with polymer (see Fig. 1a), characterized by four parameters: Δ = face-to-face interparticle spacing, g = edge-to-edge interparticle spacing, d_c = lateral dimension of particle, and h = particle height or thickness. Note that a single particle can be characterized by one or more platelets per stack. The interparticle spacing Δ can be given by

$$\Delta = \xi^2 h_0 \left(N \frac{\phi_p}{\phi_c} - \frac{d_{001}}{h_0} + 1 \right) \quad (1)$$

where ϕ_p is the polymer volume fraction, ϕ_c is the clay volume fraction, N is the number of platelets per stack ($N \geq 1$), d_{001} is the interplatelet basal spacing, h_0 is the thickness of a single platelet (≈ 1 nm), and ξ^2 is the fractional area occupied by particles in a plane: $\xi = d_c/(g + d_c)$ and $0 \leq \xi \leq 1$. For PCNs with typical clay loadings (~ 5 wt%), ϕ_p is much larger than ϕ_c, and d_{001} is less than 5 nm. In this case, $N\phi_p/\phi_c >> (d_{001}/h_0 - 1)$, and eq 1 can be approximated to

$$\Delta \approx \xi^2 N h_0 \phi_p/\phi \quad (2)$$

This indicates that for a given ϕ_c, Δ increases as N or ξ increases. In cases of particles with large aspect ratios or PCNs with high clay loadings (i.e., $g << d_c$), $\xi \rightarrow 1$, while ξ could be much less than 1 in PCNs with very low clay loadings. Thus, the interparticle spacing Δ is roughly proportional to the number of platelets per stack N, which was previously defined as an inverse degree of exfoliation.[16] That is, if ξ is similar, larger interparticle spacings correspond to more platelets per stack, lower exfoliation, and more particle aggregation.

For idealized PCNs containing fully exfoliated clay in which N =1, $h_0 \approx$ 1 nm and ξ = 1, polymer and clay are perfectly stratified so that minimum interparticle spacings, Δ_i, are given simply by the clay volume fraction:

$$\Delta_i = h_0 (1 - \phi_c)/\phi_c \quad (3)$$

If written as $\Delta_i = h_0/\phi_c - h_0$, it can be seen that the idealized spacing is proportional to the inverse clay volume fraction, namely, $\Delta_i \sim 1/\phi_c$ if $\phi_c << 1$ (*e.g.*, $h_0/\phi_c >> h_0$). This is consistent with experimental observations of one-dimensional swelling of a pure lamellar phase[26] and nematic aqueous suspensions of natural clay.[27] For the more commonly employed clay weight fraction, w_c:

$$\Delta_i = h_0 (\rho_c/\rho_p) (1 - w_c)/w_c \quad (4)$$

where ρ_c and ρ_p are clay and polymer densities, respectively. Such idealized interparticle spacings represent average interplatelet spacings in PCNs containing fully exfoliated and homogeneously dispersed clay.

Interparticle spacings of lamellar nanoparticulate relaxation sinks (*cf.* Fig. 1) are analytically related to NMR magnetization growth by the following expression:[18]

$$\frac{M(t)}{M_o} = 1 - \left(\frac{4D}{\beta\Delta^2}\right)^{1/2} \tan\left(\frac{\beta\Delta^2}{4D}\right)^{1/2} \exp(-t/T_{1,s}) - \frac{8}{\pi^2}\sum_{n=0}^{\infty}\frac{1}{(2n+1)^2}\left[\frac{1}{1-(2n+1)^2\pi^2 D/(\beta\Delta^2)}\right] \times \exp\left[-\left(\frac{(2n+1)^2\pi^2 D}{\Delta^2} + \frac{1}{T_{1,m}}\right)t\right] \quad (5)$$

where M_0 is the total equilibrium magnetization, D is the bulk spin diffusion coefficient (uniform, not a function of spatial position), $1/T_{1,m}$ is the bulk matrix nuclear relaxation rate, $1/T_{1,s}$ is the relaxation rate of the clay surface nuclei, and β is the difference between $1/T_{1,s}$ and $1/T_{1,m}$ (i.e., $\beta = 1/T_{1,s} - 1/T_{1,m}$). It was assumed that $\Delta >> 2b$, where b is the thickness of the clay surface layer (*e.g.*, ~ 0.4 nm reported previously[15, 16]) (*cf.* Fig. 1b).

The paramagnetic contribution to the overall longitudinal relaxation rate, $R_{1,para}$ is computed: $R_{1,para} = 1/T_{1,PCN} - 1/T_{1,m}$, where $1/T_{1,PCN}$ is the relaxation rate of the PCN, [15, 21] and the relaxation rate, $1/T_{1,m}$ of the matrix is often taken to be the relaxation rate, $1/T_{1,polymer}$ of the pure polymer.[14, 16, 21, 28] Using eq 5, we calculated magnetization growth profiles for nanocomposites with D = 0.7 nm^2/ms, $T_{1,m}$ = 1.635 s, $T_{1,s}$ = 5 ms, and for a range of interparticle spacings (IPS) between 15 and 100 nm, typical IPS dimensions in technically relevant PCNs. These are shown in Figure 2(a). With increasing IPS, magnetization growth is delayed. These calculated curves were also plotted as $\ln(1 - \langle M(t)/M_o \rangle)$ versus recovery time, t, from which the $T_{1,PCN}$ values were determined from the slopes (*cf.* ESI†, Fig. S1). Figure 2(b) shows the resulting $R_{1,para}$ as a function of IPS. The paramagnetic contribution to the NMR relaxation rate, $R_{1,para}$ decreases monotonically with increasing interparticle spacing. A scaling relation is given by

$$R_{1,para} \sim \Delta^{-2} \quad (6)$$

This scaling behavior, embodied in eq 5 and consistent with numerical calculations by VanderHart, et al.,[15] is a consequence of

the paramagnetic relaxation enhancement being controlled by spin diffusion.

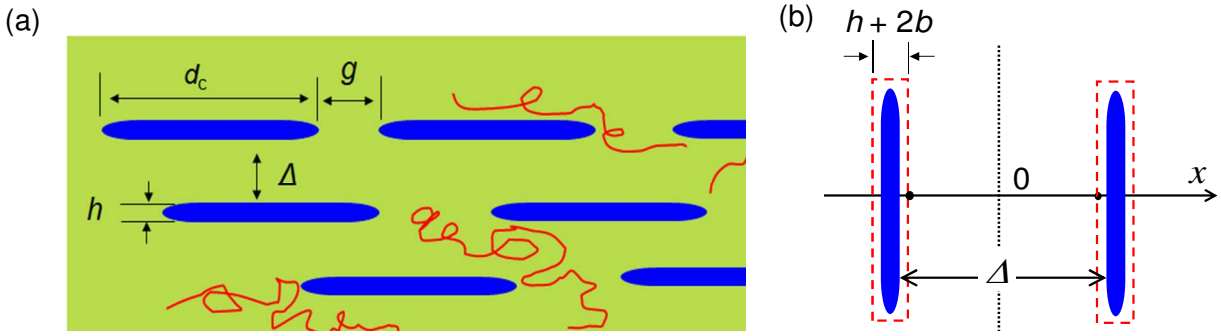

Fig. 1 (a) Schematic of polymer-clay nanocomposite with stratified clay particles characterized by face-to-face interparticle separation Δ, thickness h, lateral dimension d_c, and edge-to-edge separation g. (b) One-dimensional lamellar model for the face-to-face domains between a pair of clay particles, where b is the thickness (≈ 0.4 nm) of the thin layer of nuclei relaxed directly by the paramagnetic centers in the clay. Clay particles can be single platelets or stacks of platelets depending on the degree of exfoliation.

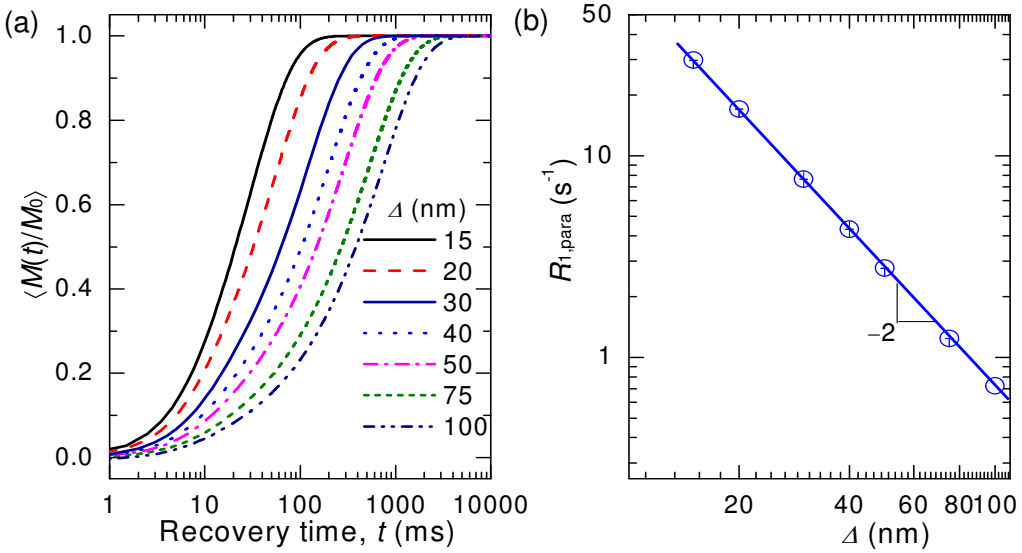

Fig.2 (a) Normalized magnetization versus recovery time calculated using eq 5 for D = 0.7 nm^2/ms, $T_{1,m}$ = 1.635 s, $T_{1,s}$ = 5 ms and different values. (b) Paramagnetic contribution to the overall spin-lattice relaxation rate $R_{1,para}$ versus interparticle spacing Δ. $R_{1,para}$ was calculated from $R_{1,para} \approx 1/T_{1,PCN} - 1/T_{1,m}$, in which the relaxation time ($T_{1,PCN}$) was determined from a linear fit of $\ln(1 - \langle M(t)/M_0 \rangle)$ versus time t, plotted from the same data shown in (a) (cf. ESI†, Fig. S1). The plot of the resulting $R_{1,para}$ as a function of Δ shows $R_{1,para} \sim \Delta^{-2}$.

When the relaxation at the clay surface is infinitely fast (i.e., $T_{1,s} \rightarrow 0$), eq 5 can be simplified and it can be shown that $R_{1,para}$ is directly proportional to Δ^{-2} (*cf.* ESI†, Model Analysis). However, as $T_{1,s}$ rises or Δ decreases (i.e., as the exfoliated particle concentration is increased), analysis of the model reveals the scaling relation in eq 6 is less valid. For typical values of Δ (50 - 100 nm, corresponding to completely exfoliated clay at 5 to 2.5 wt%, respectively) and $T_{1,s}$ (< 25 ms), the scaling relation in eq 6 is reasonably valid and useful. This is illustrated in Figure 3 for simulations using different $T_{1,s}$ values. The scaling relation of eq 6 holds, that is, the log-log plot of $R_{1,para}$ versus Δ shown in Figure 3 exhibits a straight line with slope = -2, for $T_{1,s}$ values ≤ about 25 ms and Δ values ≥ approximately 30 nm (corresponding to completely exfoliated clay at ≤ 8 wt%). For small Δ, direct dipolar interactions between the paramagnetic centers and adjacent nuclei cannot be neglected, while eq 5 neglects these with the assumption that $\Delta >> 2b$. The magnetization growth is thus controlled by direct relaxation of surface nuclei rather than by spin diffusion,[14,31] and the scaling relation of eq 6 does not hold.

In practice, we expect the scaling relation, $R_{1,para} \sim \Delta^{-2}$ to be valid for most technically relevant PCNs containing typical amounts of paramagnetic clay. First of all, the relaxation rate of clay surface nuclei ($T_{1,s}$), which strongly depends on the concentration of paramagnetic ions due to the electron-nucleus coupling,[16, 24, 28, 29] is much shorter than that of neat polymer. In widely studied MMTs (*e.g.*, from Southern Clay Products, typically containing ~5 wt% Fe_2O_3), clay surface nuclei exhibit $T_{1,s}$ values on the order of a few

milliseconds at magnetic fields up to several hundred MHz,[15, 16] while the bulk polymer T_1 is hundreds of milliseconds or even longer. Secondly, in typical PCNs, large average interparticle spacings (*e.g.*, > 10 nm) have been often observed at clay concentrations < 20 wt%. For instance, the average Δ is larger than the idealized spacing, $\Delta_i \approx 23$ nm (*cf.* eqs 3 and 4) in 10 wt% MMT nanocomposites due to the presence of clay particle aggregates.[30]

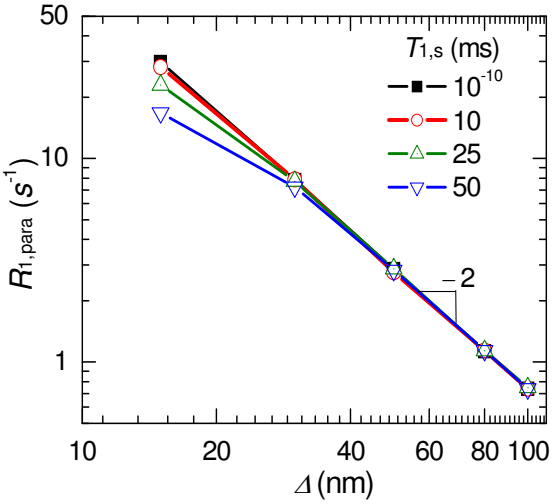

Fig.3 Paramagnetic contribution to the overall spin-lattice relaxation rate, $R_{1,para}$ versus interparticle spacing Δ for D = 0.7 nm^2/ms, $T_{1,m}$ = 1.635 s, and different $T_{1,s}$ values. The normalized magnetization profiles were first simulated using eq 5, and then the plots of $R_{1,para}$ versus Δ were calculated as shown in Figure 2(b). The slope of -1 is for the simulated data from Δ = 15 to 30 nm using $T_{1,s}$ = 50 ms.

Average interparticle separations (Δ) determined from experimental $R_{1,para}$ values can be compared to idealized interparticle separations (Δ_i) calculated from clay content (*cf.* eqs 3 and 4) and a measure of dispersion can be defined:

$$\alpha = \Delta_i / \Delta \quad (7)$$

Values for α depend on the degree of exfoliation, stratification and homogeneity of clay particle distribution. In general, dispersion quality decreases as α decreases and approaches 0. Substituting from eqs 2 and 3 leads to the following expression for α:

$$\alpha \approx N^{-1}\xi^{-2} \quad (8)$$

in which the relation to the degree of exfoliation is explicit through N, the number of platelets per stack, and to the dispersion homogeneity through ξ, the fractional area occupied by particles. Thus, even if the clay remains fully exfoliated (*e.g.*, N = 1) upon increasing clay content, ξ could increase leading to a decrease in α. However, given the large aspect ratio (d_c/h ~ 30 to 1000) [9, 16, 31] and surface area (~750 m^2/g) [32] of montmorillonite, N is expected to influence α more than ξ in PCNs filled with a typical concentration of clay particles.

By incorporating α as a measure of dispersion into eq 6, we redefine the scaling relation:

$$R_{1,para} \sim \alpha^2 \Delta_i^{-2} \quad (9)$$

According to eq 9, plotting $R_{1,para}$ versus Δ_i^{-2} should yield straight lines when clay dispersion is of similar quality, that is, α is constant. Deviation from such lines will provide insight into how the quality changes with clay concentration. For fully exfoliated and highly dispersed clay, lines can be assigned slopes containing α = 1. When aggregation of platelets leads to dispersions characterized by interparticle separations that are twice the size of the fully exfoliated case, that is, $\alpha = \Delta_i/\Delta = 1/2$, slopes of these plots will predictably decrease by $\alpha^2 = 1/4$. These plots should be useful for visualizing quality of clay dispersion as clay content increases.

Alternatively, we can substitute eq 4 into eq 9 and combine constants to yield a direct relationship between $R_{1,para}$ and the clay weight fraction, w_c:

$$R_{1,para} \sim h_0^{-2}(\rho_p/\rho_c)^2\alpha^2 w_c^2/(1 - w_c)^2 \quad (10)$$

Equation 10 shows that the paramagnetic contribution to the longitudinal NMR relaxation rate, $R_{1,para}$ is correlated with clay weight fraction, w_c through the extent of exfoliation, α; more simply, $R_{1,para} \sim \alpha^2 [(1/w_c) - 1]^{-2}$. Plots of $R_{1,para}$ versus w_c should yield curves of constant dispersion quality, the relative magnitude of which is proportional to α^2. As dispersion quality increases, $R_{1,para}$ increases.

According to eqs 9 and 10, we can calculate the relative magnitude of $R_{1,para}$ versus Δ_i or w_c for a given series of polymer-clay nanocomposites measured at a given magnetic field strength. With independent knowledge of the dispersion state of a single sample obtained from other experimental methods such as X-ray diffraction (XRD) or TEM, these NMR-determined relative exfoliation values can be adjusted to provide absolute measures of the dispersion (*i.e.*, α) for all of the samples. We have already shown that $R_{1,para}$ contains information on the distribution of interparticle spacings.[18] Thus, the scaling method described here and embodied in eqs 9 and 10 can be used to quantify exfoliation as platelets/stack if all of the samples of a given series exhibit similar dispersion homogeneity. Otherwise, the scaled quantity α reflects the overall dispersion quality as indicated in eq 8. The advantage of this scaling approach is that it precludes the need for conducting TEM, image analysis, and statistical analysis of the images on a large number of samples, which saves time. NMR results are naturally averaged values over the sample. In the following, we demonstrate how the scaling relations of eqs 9 and 10 can be used to explore and visualize clay exfoliation and dispersion quality in polymer/clay nanocomposites.

Poly(vinyl alcohol)/Montmorillonite Nanocomposites

A series of six poly(vinyl alcohol) (PVA)/montmorillonite (MMT) nanocomposites were prepared at < 10 wt% clay loadings. These samples were examined because they are considered model nanocomposites for verifying the scaling relations. First of all, the MMT is believed to be fully exfoliated across a broad concentration range: the XRD profile of the most concentrated sample shows no basal peak (001) at scanning angles of $2\theta \leq 2°$ (see ESI, Fig. S3†), indicating full exfoliation, or at least basal spacings, d_{001} > 4.4 nm. Secondly, the interparticle spacing in these samples should be large enough for $R_{1,para} \sim \Delta^{-2}$ to be valid (*e.g.*, for full exfoliation, Δ_i = 25 nm for the most concentrated sample of 9.1 wt% MMT, *cf.* eq 4). Lastly, the relaxation of the MMT surface nuclei is sufficiently fast compared to the bulk $T_{1,m}$ of the PVA. For instance, these PVA/MMT nanocomposites were prepared with octadecylamine-

modified STx-1b MMT (C18-MMT_{STx-1b}) with d_{001} = 1.84 nm (see ESI, Fig. S3†). The measured T_1 of the observable ^{1}Hs on this clay surface is ~21 ms at 300 MHz (see ESI, Fig. S4†), which is much shorter than the $T_{1,m}$ = 11640 ms of PVA.

Figure 4 shows $R_{1,para}$ versus (a) Δ_i^{-2} (calculated using eq 4) and (b) w_c for a series of six PVA/MMT_{STx-1b} nanocomposites (1.2 wt% Fe_2O_3 in MMT_{STx-1b}). For all clay contents, $R_{1,para}$ is linearly proportional to Δ_i^{-2} (Fig. 4a), consistent with eq 9, and consistent with the curve predicted by eq 10 when plotted versus w_c (Fig. 4b). Both representations indicate that clay dispersion in these samples is of similar quality with increasing clay concentration. This is consistent with the initial slopes of the magnetization growth curves[14,16,23] for these samples (see ESI, Fig. S5†), and also with reported TEM and X-ray diffraction data for other PVA/MMT nanocomposites.[19, 20] Assuming these samples are fully exfoliated and the dispersion homogeneity does not change appreciably with increasing clay concentration, we have labelled the straight line in Fig. 4(a) and the solid curve in Fig. 4(b) as $\alpha = 1$. This value of $\alpha = 1$ represents an average number of platelets/stack, N = 1 and the fractional area occupied by particles in a plane, $\xi \approx 1$ (*cf.* eq 8). We then used eqs 9 and 10 to predict the scaling of $R_{1,para}$ versus Δ_i^{-2} and w_c, respectively, for when the average interparticle spacing is twice that shown for a fully exfoliated sample (*i.e.*, when N = 2, $\alpha = 0.5$). In Figure 4, this scaling prediction is shown as a dot-dashed line (a), and curve (b). The data points for these fully exfoliated samples are more consistent with the α = 1 line than with the $\alpha = 0.5$ line. These results indicate that for polymer/clay nanocomposites containing large interparticle spacings, sufficiently fast relaxation sinks and consistent dispersion homogeneity, the NMR relaxation behavior can be described by the scaling relations: $R_{1,para} \sim \alpha^2 \Delta_i^{-2}$ (eq 9) and $R_{1,para} \sim \alpha^2 w_c^2 / (1 - w_c)^2$ (eq 10).

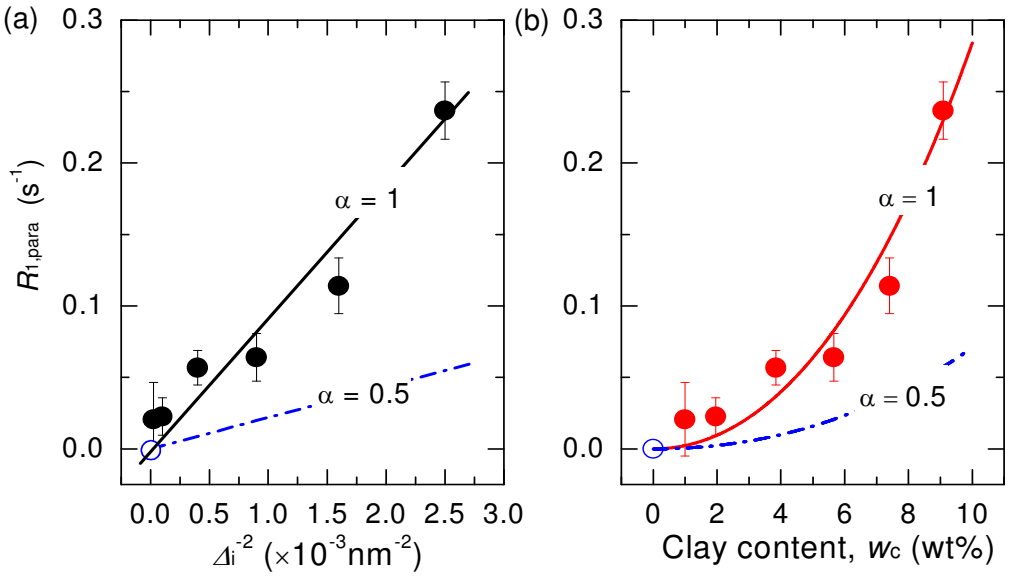

Fig.4 Paramagnetic contribution to the spin-lattice relaxation rate, $R_{1,para}$, versus (a) inverse ideal interparticle separation squared, Δ_i^{-2} (*cf.* eqs 4 and 9), and (b) clay content, w_c (wt %) (*cf.* eq 10), for a series of PVA/MMT_{STx-1b} nanocomposites where the MMT_{STx-1b} contains 1.2 wt% Fe^{3+} as Fe_2O_3. The α values on the lines are inversely related to average number of platelets/stack (N) and the dispersion homogeneity (ξ): $\alpha \approx N^{-1}\xi^{-2}$ (eq 8). Solid line is (a) linear and (b) curvilinear fit through all MMT_{STx-1b} concentrations and the zero point; it represents fully exfoliated samples with N = 1 as long as the dispersion homogeneity remains constant. Dot-dashed lines were drawn for samples with an average number of platelets/stack, N = 2 (α = 1/2) by scaling the slope of the solid lines ($\propto \alpha^2$, *cf.* eqs 9 and 10) by 1/4.

Nylon 6/MMT Nanocomposites

Application of the scaling relations are demonstrated on an experimental data set for some technically relevant samples, nylon 6/MMT nanocomposites.[21] The data for these samples exhibit trends far from the ideal scenario demonstrated above for PVA/MMT_{STx-1b} nanocomposites. However, the samples are well characterized by various experimental methods. While XRD can be used to rapidly determine whether clay particles are exfoliated or not, statistical analysis of TEM images, costly in terms of time, can provide much more information. Such TEM data, along with NMR relaxation times, have been reported by van Es and Bertmer, *et al.*[21, 25] for nylon 6/MMT nanocomposites with clay contents between 0.2 and 20 wt %. From their TEM data, they concluded that in the 5 wt% sample, "the majority of clay exists in groups consisting of two platelets still stuck together."[21] Thus, using this sample as the reference (platelets/stack = 2, $\alpha = 0.5$), we show $R_{1,para}$ versus Δ_i^{-2} in Figure 5. We assume that all samples exhibit similar dispersion homogeneity at clay contents ≥ 2.5 wt%. After fitting a reference line for the 5 wt% sample (solid line, N = 2, $\alpha = 0.5$), lines marked N = 1, 3 and 4 were drawn with slopes ($\propto \alpha^2$, *cf.* eq 9) that are 4, 4/9, and 1/4 times the reference slope, respectively. From the plot it is directly revealed how the exfoliation degrades with increasing clay concentration from full exfoliation at 1 wt % to larger particles with an average number of platelets/stack greater than three at 20 wt %. At 2.5 wt %, the average number of platelets per particle is about

1.5, entirely consistent with the reported analysis of TEM data that shows about half of the particles are fully exfoliated while the rest contain stacks of 2 – 3 platelets.[21]

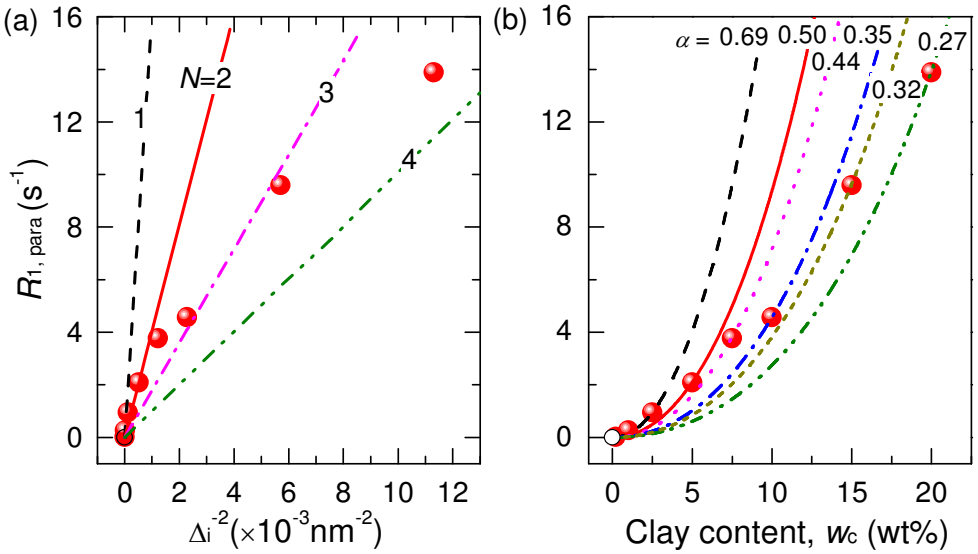

Fig.5 Paramagnetic contribution to the spin-lattice relaxation rate, $R_{1,para}$, versus (a) inverse ideal interparticle separation squared, Δ_i^{-2} (cf. eqs 4 and 9), and (b) clay content w_c (*cf.* eq 10), for a series of nylon 6/MMT nanocomposites filled with MMT containing Fe^{3+} (3.11 wt % as Fe_2O_3).[21, 25] Relaxation times were measured at 500 MHz.[21] Numbers on lines in (a) denote average number of platelets/stack (*N*). The solid line ($N = 2$) was chosen as the reference line for the 5 wt% sample since TEM data indicated the majority of clay particles consisted of 2 platelets/stack. Lines marked with $N = 1$, 3 and 4 were derived by scaling the reference slope ($\propto \alpha^2$, *cf.* eq 9) by 4, 4/9 and 1/4, respectively. The α values in (b) ($\alpha \approx N^{-1}\xi^{-2}$, *cf.* eq 8) were determined by fitting individual data points to eq 10.

In Figure 5(b), $R_{1,para}$ is plotted versus w_c. Curves are calculated for each clay concentration ≥ 2.5 wt% MMT using eq 10. The α values obtained directly from these predictions are shown on the curves. As clay content increases, α values, which reflect the relative quality of clay dispersion, decrease. Again, using the 5 wt % sample as a reference for which we know contains predominantly 2 platelets/stack ($\alpha = 0.5$), we can scale all other α values to quantify dispersion for all samples. These α values are plotted in Figure 6 versus clay content. The most dilute samples (0.2 and 1 wt % MMT) are defined to have $\alpha = 1$ since TEM indicates complete exfoliation and homogeneous distribution. However, the α values for these two samples are not simply explained by the degree of exfoliation because TEM shows that the edge-to-edge interparticle distance is not negligible as compared to Δ; that is, ξ is not equal to 1. Moreover, samples containing very low clay concentrations do not satisfy the requirements of the model (*cf.* eq 5, Fig. 1), namely that the spin diffusion length, $(5T_{1,PCN}\ D)^{1/2}$ is greater than half the interparticle separation and the samples are likely far from perfectly stratified. For these two samples, the spin diffusion lengths are calculated using $D = 0.7$ nm^2/ms to be 74 and 63 nm, respectively, which are much smaller than half the calculated Δ_i (*cf.* eq 4) or reported Δ_{TEM} values.

For the most concentrated systems, for example 15 and 20 wt% MMT, surfactants in commercial MMT (> 9 wt% of the PCN) may alter the relaxation behavior of the bulk polymer too much from that of the neat polymer to yield sufficiently accurate $R_{1,para}$ values, since the $R_{1,para}$ calculation assumes $T_{1,m} = T_{1,polymer}$. Furthermore, the scaling relations may break down for small Δ (*cf.* Fig. 3). The TEM images reveal very small interparticle spacings at high clay contents (*e.g.*, $\Delta = 7$ and 4 nm at 15 and 20 wt%, respectively), when compared with the dilute samples.[21, 25] Note that ξ values may also increase as clay content increases, leading to an overestimate of the α value at higher clay concentrations (assuming α is being used as a measure of exfoliation only). This, however, is not the case for these nylon/MMT samples as TEM shows similar ξ values for clay concentrations ≥ 2.5 wt%.[21]

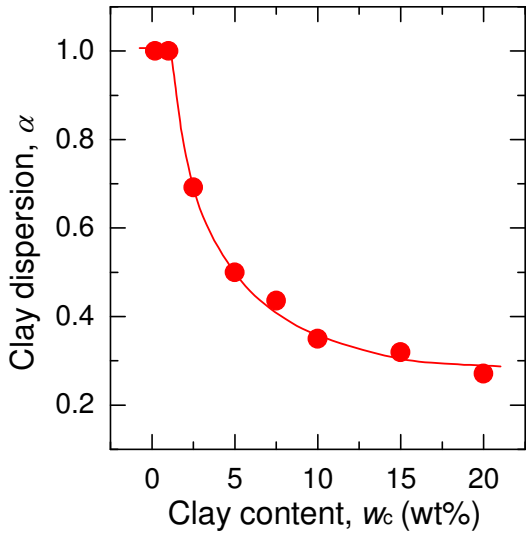

Fig. 6 Clay dispersion, α ($\alpha \approx N^{-1}\xi^{-2}$, *cf.* eq 8), versus clay content, w_c, for nylon 6/MMT nanocomposites with varying clay content. The α values were calculated by fitting $R_{1,para}$ values to eq 10 as shown in Figure 5(b). As discussed in the text, the most dilute samples (0.2 and 1 wt% MMT) do not satisfy the model requirements and are therefore assigned to $\alpha = 1$ since TEM

shows that the clay in these samples is completely exfoliated and homogeneously dispersed.[21]

Figure 6 shows that clay dispersion decreases upon increasing clay content, in particular, when $w_c \leq 10$ wt%. The reduction can be attributed to aggregation and formation of tactoids, as observed in TEM images.[21, 25] The analysis that leads to results like those shown in Figure 6 begins with a model in which the paramagnetic contribution to the spin-lattice relaxation rate ($R_{1,para}$) is indirectly proportional to the average interparticle separation squared. Conversely, when $R_{1,para}$ is assumed to be directly proportional to the surface-to-volume ratio of clay to polymer,[21] results can be derived in which the dispersion quality appears to improve with increasing clay content (Figure 2 in reference[21]). Bourbigot *et al*. showed that surface-to-volume ratios of clay to polymer are directly proportional to initial slopes of relaxation recovery curves, not $R_{1,para}$.[14] Since initial slopes of relaxation recovery curves yield surface-to-volume ratios of clay to polymer they will also provide degrees of exfoliation. Paramagnetic contributions to the overall spin-lattice relaxation rate provide information on the overall dispersion quality, which depends on both degree of exfoliation and dispersion homogeneity (*cf*. eq 8).

Conclusions

From a previously developed analytical solution of a lamella-based model for describing NMR longitudinal relaxation in polymer nanocomposites filled with paramagnetic clay, scaling relations were derived. The paramagnetic contribution to the relaxation rate, $R_{1,para}$ was found to be inversely proportional to the square of the interparticle spacing and directly proportional to the weight fraction squared. These scaling relations are valid for large interparticle spacings (*e.g*., $\Delta > 10$ nm), sufficiently fast relaxation of clay surface nuclei relative to that of polymer matrix nuclei (*e.g*., $T_{1,s} << T_{1,m}$), and consistent dispersion homogeneity. We defined a relative measure of clay dispersion, α, as the ratio of idealized interparticle separation to the actual separation; α is correlated with the degree of exfoliation and dispersion homogeneity. Use of the scaling relations depends on knowledge of the clay dispersion in at least one sample determined from an independent measurement such as TEM. The scaling relations were validated by comparison with data obtained for a series of well exfoliated poly(vinyl alcohol)/montmorillonite (PVA/MMT) nanocomposites. We further demonstrated the utility of these scaling relations by examining clay dispersion in a series of technically relevant nylon 6/MMT nanocomposites, for which the results agree with TEM data. The α values can be determined by calculating curves for $R_{1,para}$ versus clay content. The scaling relations presented in this paper provide a simple formalism to analyze the dispersion quality of clay particles in polymer-clay nanocomposites based on NMR T_1 relaxation data, which generally can be measured for bulk samples within a few minutes.

Acknowledgements

Funding for this work was granted by the National Science Foundation (DMR-0710501). The authors are indebted to Dr. Marko Bertmer from Leipzig University for kindly providing NMR relaxation data and other information related to their studies. The authors also express their sincere thanks to Southern Clay Products for providing supporting data.

[a]School of Materials Science and Engineering, Georgia Institute of Technology, 801 Ferst Drive, Atlanta, GA 30332 USA.
[b]School of Chemistry and Biochemistry, Georgia Institute of Technology, 901 Atlantic Drive, Atlanta, GA 30332 USA.
*E-mail: bxu6@gatech.edu; beckham@gatech.edu

†Electronic Supplementary Information (ESI) available. See DOI: 10.1039/b000000x/

Notes and References

1 B. Chen, J. R. G. Evans, H. C. Greenwell, P. Boulet, P. V. Coveney, A. A. Bowden, A. Whiting, *Chem. Soc. Rev.* 2008, **37**, 568-594.
2 L. J. Bonderer, A. R. Studart, L. J. Gauckler, *Science* 2008, **319**, 1069-1073.
3 A. K. Kaushik, P. Podsiadlo, M. Qin, C. M. Shaw, A. M. Waas, A. N. Kotov, E. M. Arruda, *Macromolecules* 2009, **42**, 6588–6595.
4 X. Zhang, L. S. Loo, *Macromolecules* 2009, **42**, 5196–5207.
5 H. D. Wagner, *Nat. Nanotech.* 2007, **2**, 742-744.
6 P. Podsiadlo, A. K. Kaushik, E. M. Arruda, A. M. Waas, B. S. Shim, J. D. Xu, H. Nandivada, B. G. Pumplin, J. Lahann, A. Ramamoorthy, N. A. Kotov, *Science* 2007, **318**, 80-83.
7 E. Manias, *Nat Mater* 2007, **6**, 9-11.
8 S. M. Liff, N. Kumar, G. H. McKinley, *Nature Mater.* 2007, **6**, 76–83.
9 B. Xu, Q. Zheng, Y. H. Song, Y. Shangguan, *Polymer* 2006, **47**, 2904-2910.
10 Z. Y. Tang, N. A. Kotov, S. Magonov, B. Ozturk, *Nat Mater* 2003, **2**, 413-U418.
11 T. D. Fornes, D. R. Paul, *Polymer* 2003, **44**, 4993-5013.
12 C. W. Chiu, C. C. Chu, S. A. Dai, J. J. Lin, *J. Phys. Chem. C* 2008, **112**, 17940-17944.
13 J. H. Rouse, S. T. White, G. S. Ferguson, *scanning* 2004, **26**, 131-134.
14 S. Bourbigot, D. L. Vanderhart, J. W. Gilman, W. H. Awad, R. D. Davis, A. B. Morgan, C. A. Wilkie, *J. Polym. Sci., Part B: Polym. Phys.* 2003, **41**, 3188-3213.
15 D. L. Vanderhart, A. Asano, J. W. Gilman, *Chem. Mater.* 2001, **13**, 3796-3809.
16 B. Xu, J. Leisen, H. W. Beckham, R. Abu-Zurayk, E. Harkin-Jones, T. McNally, *Macromolecules* 2009, **42**, 8959-8968.
17 R. Graf, M. R. Hansen, D. Hinderberger, K. Muennemanna, H. W. Spiess, *Phys. Chem. Chem. Phys.* 2014, **16**, 9700-9712.
18 B. Xu, J. Leisen, H. W. Beckham, *Nanoscale* 2014, **6**, 1318–1322.
19 A. Asano, M. Shimizu, T. Kurotsu, *Chem. Lett.* 2004, **33**, 816-817.
20 K. E. Strawhecker, E. Manias, *Chem. Mater.* 2000, **12**, 2943-2949.
21 M. Bertmer, M. F. Wang, M. Kruger, B. Blumich, V. M. Litvinov, M. van Es, *Chem. Mater.* 2007, **19**, 1089-1097.
22 A. R. Mermut, A. F. Cano, *Clays Clay Miner.* 2001, **49**, 381-386.
23 Q. Zheng, B. Xu, Y. H. Song, H. M. Yang, Y. Pan, *J Mater. Res.* 2005, **20**, 357-363.
24 B. Xu, J. Leisen, U. Boehme, U. Scheler, H. W. Beckham, *Z. Phys. Chem.* 2012, **226**, 1229–1241.
25 M. Van Es, Ph.D. thesis, Technische Universiteit Delft, (Delft), **2001**.
26 J.-C. P. Gabriel, F. Camerel, B. J. Lemaire, H. Desvaux, P. Davidson, P. Batail, *Nature* 2001, **413**, 504-508
27 L. J. Michot, I. Bihannic, S. Maddi, S. S. Funari, C. Baravian, P. Levitz, P. Davidson, *PNAS* 2006, **103**, 16101–16104.
28 C. Calberg, R. Jerome, J. Grandjean, *Langmuir* 2004, **20**, 2039-2041.
29 D. L. VanderHart, A. Asano, J. W. Gilman, *Chem. Mater.* 2001, **13**, 3781-3795.
30 Z. P. Luo, J. H. Koo, *Polymer* 2008 **49**, 1841-1852.
31 B. Q. Chen, J. R. G. Evans, *Macromolecules* 2006, **39**, 1790-1796.
32 A. E. Blum, D. D. Eberl, *Clays and Clay Minerals* 2004, **52**, 589-602.

Title

Nanoparticle Dispersion in Polymer Nanocomposites by Spin-Diffusion-Averaged Paramagnetic Enhanced NMR Relaxometry: Scaling Relations and Applications

Bo Xu, Johannes Leisen and Haskell W. Beckham**

The table of contents

Scaling relations were identified between NMR relaxometric observables and nanoparticle contents/spacings that enable predictions of clay dispersion in polymer nanocomposites.

for Table of Contents use only

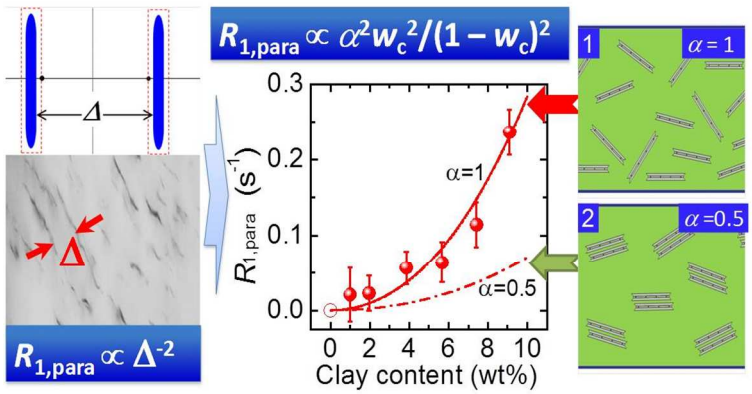

Electronic Supplementary Material (ESI) for PCCP

Supporting Information for

Nanoparticle Dispersion in Polymer Nanocomposites by Spin-Diffusion-Averaged Paramagnetic Enhanced NMR Relaxometry: Scaling Relations and Applications

Bo Xu,[*a] *Johannes Leisen*[b] *and Haskell W. Beckham*[*a]

[a]*School of Materials Science and Engineering, Georgia Institute of Technology, 801 Ferst Drive, Atlanta, GA 30332 USA. E-mail: bxu6@gatech.edu; beckham@gatech.edu*

[b]*School of Chemistry and Biochemistry, Georgia Institute of Technology, 901 Atlantic Drive, Atlanta, GA 30332 USA*

This file contains:

(1) Proton NMR longitudinal relaxation curves for a series of PVA/$MMT_{STx\text{-}1b}$ nanocomposites (Figure S1)

(2) Model analysis: sinks with infinitely fast relaxation (Figure S2)

(3) X-ray diffraction patterns of octadecylamine-modified $MMT_{STx\text{-}1b}$ and a PVA/$MMT_{STx\text{-}1b}$ nanocomposite (PVA/$MMT_{STx\text{-}1b}$ = 100/10, w/w) (Figure S3)

(4) Proton NMR longitudinal relaxation curve for the octadecylamine-modified $MMT_{STx\text{-}1b}$ (Figure S4)

(5) Initial relaxation in a series of PVA/$MMT_{STx\text{-}1b}$ nanocomposites (Figure S5)

References

*Corresponding authors. E-mail: bxu6@gatech.edu; beckham@gatech.edu

Electronic Supplementary Material (ESI) for PCCP

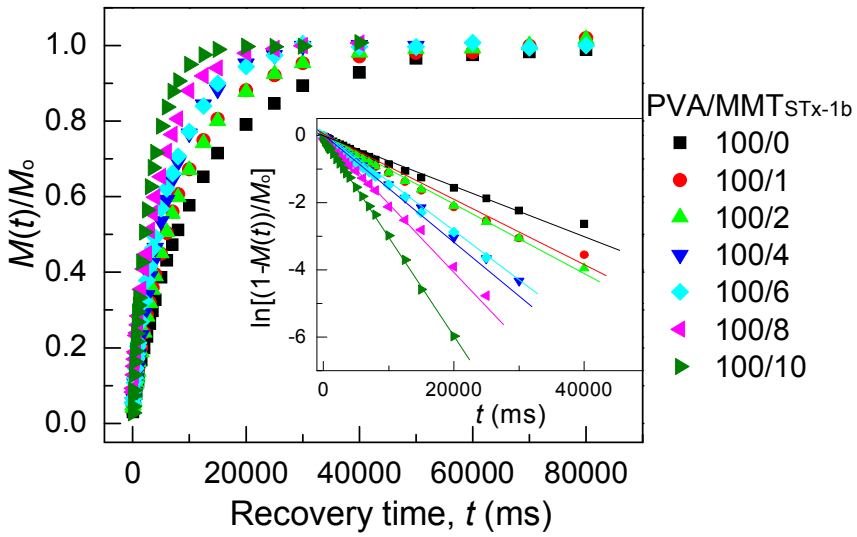

Figure S1. Normalized magnetization, $M(t)/M_o$, versus recovery time, t for poly(vinyl alcohol)/montmorillonite (PVA/$MMT_{STx\text{-}1b}$) nanocomposites at weight ratios (PVA/$MMT_{STx\text{-}1b}$) of 100/1, 100/2, 100/4, 100/6, 100/8, and 100/10. The inset displays the same data plotted as $\ln[1 - M(t)/M_o]$ versus recovery time, t, the slopes of which reflect the inverse T_1s. The relaxation rate increases upon increasing the $MMT_{STx\text{-}1b}$ content; all nanocomposites exhibit faster relaxation (shorter T_1^H) than the corresponding pure PVA. The calculated T_1 values are 11.64 ± 0.23 s, 9.38 ± 0.23 s, 9.21 ± 0.11 s, 7.01 ± 0.0.07 s, 6.67 ± 0.12 s, 5.00 ± 0.11 s and 3.10 ±0.23 s for weight ratios from 100/1 to 100/10, respectively.

Model analysis: sinks with infinitely fast relaxation

As discussed in the main text, we recently reported an analytical relationship between NMR magnetization growth and interparticle spacings (IPS) in lamellar polymer/paramagnetic clay nanocomposites:[1]

$$\frac{M(t)}{M_o} = 1 - \left(\frac{4D}{\beta\Delta^2}\right)^{1/2} \tan\left(\frac{\beta\Delta^2}{4D}\right)^{1/2} \exp(-t/T_{1,s}) - \frac{8}{\pi^2}\sum_{n=0}^{\infty}\frac{1}{(2n+1)^2}\left[\frac{1}{1-(2n+1)^2\pi^2 D/(\beta\Delta^2)}\right]\exp\left[-\left(\frac{(2n+1)^2\pi^2 D}{\Delta^2}+\frac{1}{T_{1,m}}\right)t\right] \quad (5)$$

Electronic Supplementary Material (ESI) for PCCP

where M_0 is the total equilibrium magnetization, D is the bulk spin diffusion coefficient (uniform, not a function of spatial position), $1/T_{1,m}$ is the bulk matrix nuclear relaxation rate, $1/T_{1,s}$ is the relaxation rate of the clay surface nuclei, and β is the difference between $1/T_{1,s}$ and $1/T_{1,m}$ (i.e., $\beta = 1/T_{1,s} - 1/T_{1,m}$). In the case of the sinks with infinitely fast relaxation (e.g., $T_{1,s} \rightarrow 0$, i.e., $\beta \rightarrow \infty$), we can simplify eq 5:

$$\frac{M(t)}{M_o} = 1 - \sum_{n=0}^{\infty} \beta_n^{-1} \exp\left[-\left(\frac{8\beta_n D}{\Delta^2} + \frac{1}{T_{1,m}}\right)t\right] \quad \text{(S1)}$$

where $\beta_n = (2n + 1)^2\pi^2/8$. The summation in eq S1 converges quite rapidly with n; numerical calculation using just two iterations yields errors less than 5% (see Figure S2). Taking only the first term of the summation, equation S1 can be recast:

$$\frac{M(t)}{M_o} = 1 - \frac{8}{\pi^2} f(t) \exp\left[-\left(\frac{\pi^2 D}{\Delta^2} + \frac{1}{T_{1,m}}\right)t\right] \quad \text{(S2)}$$

where $f(t) = 1 + 1/9 \exp(-8B\ t) + 1/25 \exp(-24B\ t) + \ldots$, and $B = \pi^2 D/\Delta^2$. The value of $f(t)$ approaches 1 if $t > (8B)^{-1} = 8\Delta^2/(\pi^2 D)$. Note that this approximation is valid when spin diffusion lengths, $(D \times 5T_1)^{1/2}$, are greater than interparticle separations, Δ. In other words, the interparticle distance is such that magnetization throughout the entire sample may equilibrate due to spin diffusion during the T_1 relaxation process. Thus, samples must be characterized by $T_1 > \Delta^2/(20D)$. Since this is approximately $(8B)^{-1} = 8\Delta^2/(\pi^2 D)$, eq S2 should sufficiently describe long-time relaxation behavior for $f(t) = 1$ (i.e., $n = 0$ in summation of eq S1). This was

Electronic Supplementary Material (ESI) for PCCP

confirmed by numerically generating relaxation curves for the first four n values of the summation (n = 0, 1, 2 and 3) using parameter values similar to those for a PCN with 5 wt% MMT and a spin diffusion coefficient, D = 0.7 nm^2/ms. These are shown in Figure S2(a) and reveal no difference in the long-time relaxation behavior when t > ~180 ms ≈ $8\Delta^2/(\pi^2 D)$. Although differences are observed in the short-time behavior, Figure S2(b) shows that these do not significantly affect the overall T_1 values determined from plots of $\ln[\pi^2/8(1-M(t)/M_o)]$ versus recovery time. As a result, from eq S2 with $f(t) = 1$, the observed $1/T_{1,PCN}$ can be obtained

$$\frac{1}{T_{1,PCN}} \approx \frac{\pi^2 D}{\Delta^2} + \frac{1}{T_{1,m}} \tag{S3}$$

Equation S3 can be compared to the semi-empirical equation used to compute the paramagnetic contribution to the spin-lattice relaxation rate:[2-4]

$$R_{1,para} = 1/T_{1,para} = 1/T_{1,PCN} - 1/T_{1,polymer} \tag{S4}$$

if the relaxation rate of the pure polymer, $1/T_{1,polymer}$, is taken to be the relaxation rate of the bulk polymer in the nanocomposite, $1/T_{1,m}$. In this case, the paramagnetic contribution to the relaxation is

$$R_{1,para} \approx \pi^2 D/\Delta^2 \tag{S5}$$

Thus, $R_{1,para} \sim \Delta^{-2}$, for sinks with infinitely fast relaxation (e.g., $T_{1,s} \rightarrow 0$, i.e., $\beta \rightarrow \infty$).

Electronic Supplementary Material (ESI) for PCCP

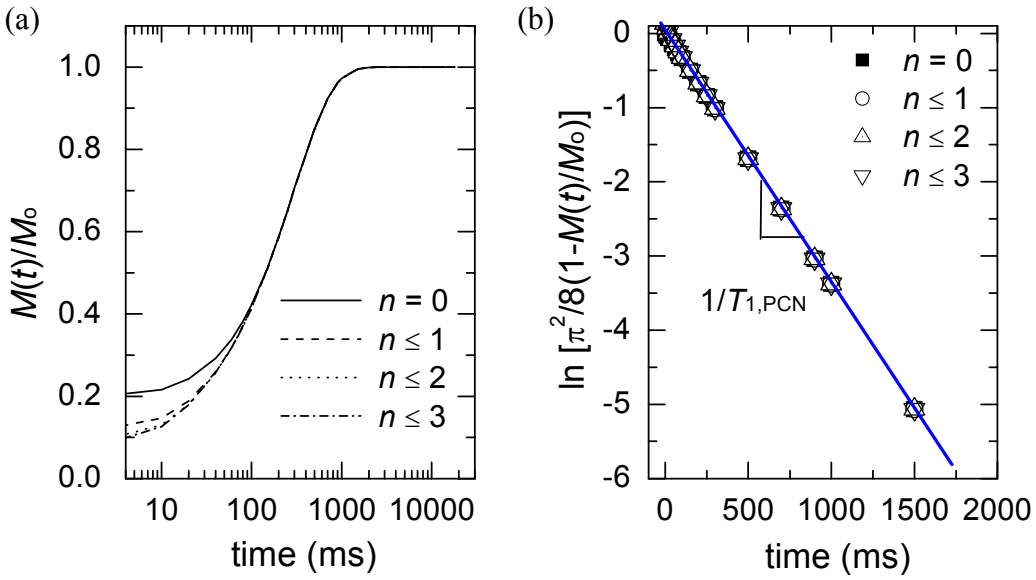

Figure S2. Relaxation curves numerically calculated using eq S1 and the first four terms of $f(t)$, corresponding to eq S2 (first term of summation only) and $n = 0$, ≤ 1, ≤ 2 and ≤ 3: (a) $M(t)/M_o$, and (b) $\ln[\pi^2/8(1 - M(t)/M_0)]$ versus recovery time. The following parameters were used in the calculation: spin diffusion coefficient, $D = 0.7$ nm^2/ms, bulk polymer relaxation time, $T_{1,m} = 1.635$ s, $\Delta = 50$ nm and recovery time range from 0.5 to 10000 ms. Calculated values of $T_{1,\,PCN}$ in (b), 296 ms ($n = 0$), 293 ms ($n \leq 1$), and 292 ms (n ≤ 2 and ≤ 3), are consistent with the relaxation constant of 296 ms determined by fitting the data points in (b) to a conventional exponential recovery.

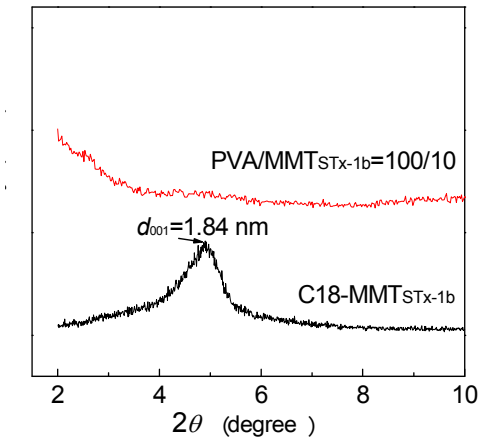

Figure S3. X-ray diffraction patterns of octadecylamine-modified $MMT_{STx\text{-}1b}$ (C18-$MMT_{STx\text{-}1b}$) and a PVA/$MMT_{STx\text{-}1b}$ nanocomposite (PVA/$MMT_{STx\text{-}1b}$ = 100/10, w/w). This PVA/$MMT_{STx\text{-}1b}$ nanocomposite contains 10 wt% clay and does not exhibit a basal peak (001) reflection, indicating the clay is exfoliated.

Electronic Supplementary Material (ESI) for PCCP

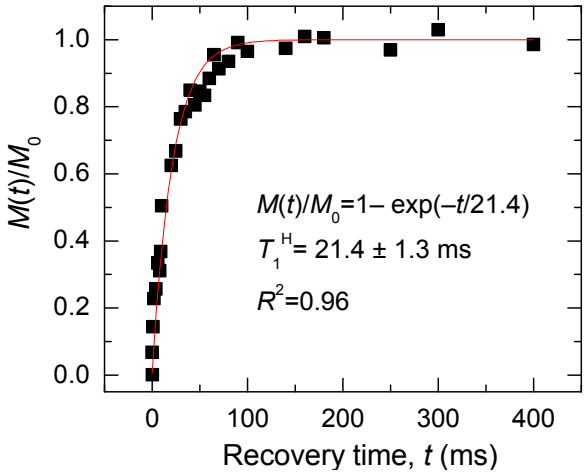

Figure S4. Normalized magnetization, $M(t)/M_o$ versus recovery time for octadecylamine-modified $MMT_{STx\text{-}1b}$ (C18-$MMT_{STx\text{-}1b}$) measured at 300 MHz. $T_1^H = 21.4 \pm 1.3$ ms.

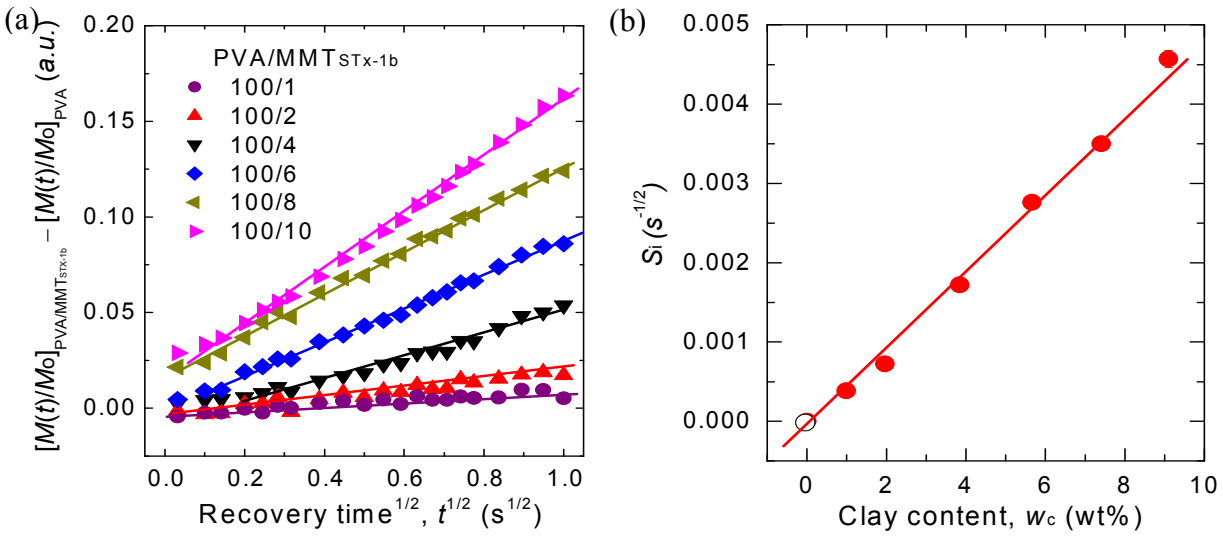

Figure S5. (a) Normalized and corrected magnetization versus the square root of recovery time for poly(vinyl alcohol)/montmorillonite ($PVA/MMT_{STx\text{-}1b}$) nanocomposites with different clay contents. $PVA/MMT_{STx\text{-}1b}$ weight ratios are $100/x$ where x = 1, 2, 4, 6, 8 and 10. The data were measured at 300 MHz and are vertically displaced to prevent overlap. Lines are linear least-square fits. Slopes of these lines, S_i are plotted in (b) as a function of clay content, w_c. These initial slopes, which reflect the effective clay/polymer interfacial area, are linearly proportional to clay weight fraction and therefore suggest similar degrees of exfoliation in these samples.

Electronic Supplementary Material (ESI) for PCCP

References

(1) Xu, B.; Leisen, J.; Beckham, H. W. Nanoparticle dispersion in polymer nanocomposites by spin-diffusion-averaged paramagnetic enhanced NMR relaxometry. *Nanoscale* **2014**, *6*, 1318–1322.

(2) Xu, B.; Leisen, J.; Beckham, H. W.; Abu-Zurayk, R.; Harkin-Jones, E.; McNally, T. Evolution of Clay Morphology in Polypropylene/Montmorillonite Nanocomposites upon Equibiaxial Stretching: A Solid-State NMR and TEM Approach. *Macromolecules* **2009**, *42*, 8959-8968.

(3) Bertmer, M.; Wang, M. F.; Kruger, M.; Blumich, B.; Litvinov, V. M.; van Es, M. Structural changes from the pure components to nylon 6-montmorillonite nanocomposites observed by solid-state NMR. *Chemistry of Materials* **2007**, *19*, 1089-1097.

(4) Calberg, C.; Jerome, R.; Grandjean, J. Solid-state NMR study of poly(epsilon-caprolactone)/clay nanocomposites. *Langmuir* **2004**, *20*, 2039-2041.